

# Robust and High Fidelity Mesh Denoising

Sunil Kumar Yadav, Ulrich Reitebuch, and Konrad Polthier

**Abstract**—This paper presents a simple and effective two stage mesh denoising algorithm, where in the first stage, the face normal filtering is done by using the bilateral normal filtering in the robust statistics framework. *Tukey's bi-weight function* is used as similarity function in the bilateral weighting, which is a robust estimator and stops the diffusion at sharp edges which helps to retain features and removes noise from flat regions effectively. In the second stage, an edge weighted Laplace operator is introduced to compute the differential coordinate. This differential coordinate helps the algorithm to produce a high quality mesh without any face normal flips and also makes the method robust against high intensity noise.

**Index Terms**—Mesh Denoising, Robust Statistics, Face normal processing, Tukey's bi-weight function, High Fidelity Mesh, Differential Coordinate.

## 1 INTRODUCTION

MESH denoising is one of the most active and fascinating research areas in geometry processing as digital scanning devices become widespread to capture the 3D points of the surface of a 3D object. In the process of data acquisition, noise is inevitable due to various internal, and external sources. Mesh denoising algorithms are focused to remove this undesired noise and compute a high quality smooth function on a triangular mesh for further use in rendering, scientific analysis, reverse engineering and medical visualization. In general, both sharp features and noise are high frequency components on the surface and are ambiguous in nature. During the surface denoising, it is a challenging task to decouple sharp features and noise, which is essential to compute a smooth surface with sharp features.

### 1.1 Related Work

In last two decades, a wide variety of smoothing algorithms have been introduced to remove undesired noise, while preserving sharp features in the geometry. For a comprehensive review on mesh denoising, readers are referred to [1], [2] and [3]. Here, an overview of current state-of-the-art methods is given, which are based on differential coordinates and bilateral filtering.

The concept of differential coordinates was initially introduced by Alexa [4] as a local shape descriptor of a geometry. Differential coordinates are able to preserve the fine details on a triangular mesh and that leads to their further applications in mesh processing, for example, Lipman et al. [5] used the same concept for mesh editing. Mesh quantization [6] and shape approximation [7] are also done by using the concept of differential coordinates. Sorkine et al. [8] introduced a general differential coordinate-based framework for mesh processing. Later, Su et al. [9] utilized differential coordinates to remove noise and compute a smooth surface.

The bilateral filtering was initially proposed by Tomasi et al. [10] for image smoothing. The relation between anisotropic diffusion [11] and bilateral filtering is explained by Barash [12]. In continuation, Black et al. [13] and Durand et al. [14] expressed anisotropic diffusion and bilateral filtering in the robust statistics framework. The concept of bilateral smoothing was extended for mesh denoising by Fleish et al. [15] and later, Jones et al. [16] explained the same concept in the robust statistics framework. Bilateral filtering was applied to the two step surface denoising method by Zheng et al. [17], where the weight functions were computed based on the normal differences (similarity measurement) and spatial distances between neighbouring faces. Later, researchers proposed a general framework for bilateral and mean shift filtering in any arbitrary domain [18]. Recently, several bilateral normal-based denoising algorithms have been published. For example, Wei et al. [19] utilized both face and vertex normals to produce a smooth surface and Yhang et al. [20] proposed a guided mesh normal filtering based on the joint bilateral filtering [21]. A tensor voting guided mesh denoising was also introduced by Wei et al. [22], where feature classification was done using the normal voting tensor and then MLS fitting was applied to remove noise.

The compressed sensing framework is also utilized to produce feature preserving mesh denoising algorithms. He et al. [23] extended the  $L^0$  image smoothing concept to a mesh denoising algorithm where the algorithm maximizes the piecewise flat regions on noisy surfaces to remove noise. The  $L^1$  optimization based algorithms were introduced by Wang et al. [24] and Wu et al. [25] where features were preserved from the residual data by the extended ROF (Rudin, Osher and Fatemi) model. In continuation, Lu et al. [26] detected features on the noisy surface using quadratic optimization and then removed noise using  $L^1$  optimization while preserving features. Later, researchers utilized the  $L^1$ -median normal filtering along with vertex preprocessing to produce a noise free surface [27]. Recently, Yadav et al. [3] proposed a binary optimization-based mesh denoising algorithm, where noise was removed by assigning the binary values to a face normal-based covariance matrix. Centin et al. [2] proposed a normal-diffusion-based mesh denoising

- Sunil Kumar Yadav, Ulrich Reitebuch and Konrad Polthier are with the Department of Mathematics and Computer Science, Freie Universität Berlin.  
E-mail: sunil.yadav@fu-berlin.de

algorithm, which removes noise components without tempering the metric quality of a surface. In this paper, a mesh denoising algorithm is introduced to provide a high fidelity mesh structure against different levels of noise without creating any normal flips.

## 1.2 Contribution

We propose a two stage mesh denoising method, where the face normal processing is mainly motivated by the robust statistics framework in anisotropic diffusion and bilateral filtering [13]. Basically, the robust statistics framework is focused on developing different estimators which are robust to outliers [28]. In the mesh denoising and robust statistic framework, sharp features are considered as the *outliers* and a proper estimator will avoid *outliers* to preserve sharp features and remove undesired noise components from a noisy surface.

We apply *Tukey's bi-weight function* for the similarity function as a robust estimator which stops the diffusion at sharp features and produces smooth umbilical regions. In the vertex update step, we use a differential coordinate-based Laplace operator along with edge-face normal orthogonality constraint. This Laplace operator is computed using the edge length as the weight function to produce a high quality mesh without face normal flips and it makes the algorithm more robust against high intensity noise.

## 2 METHOD

The proposed method is implemented in two different stages. In the first stage, noisy face normals are processed using the bilateral filtering in the robust statistics framework and in the second stage, a high fidelity mesh is reconstructed using the edge-face normal orthogonality constraint and the edge-weighted differential coordinate.

### 2.1 Robust Bilateral Face Normal Processing

In the first step of the proposed algorithm, we smooth noisy face normals using the bilateral filter, which is a non-linear filter and it computes output using the weighted average of the input:

$$\tilde{\mathbf{n}}_i = \frac{1}{K_i} \sum_{j \in \Omega_i} a_j f(|\mathbf{c}_i - \mathbf{c}_j|, \sigma_c) g(|\mathbf{n}_i - \mathbf{n}_j|, \sigma_s) \mathbf{n}_j, \quad (1)$$

where  $\mathbf{n}_j$  represents a noisy face normal and belongs to the geometric neighbour disk  $\Omega_i$  of the central face normal  $\mathbf{n}_i$ . The geometric neighborhood is more robust against non-uniform meshes compared to the combinatorial neighborhood [3]. The normalization factor  $K_i$  is defined as:

$$K_i = \sum_{j \in \Omega_i} a_j f(|\mathbf{c}_i - \mathbf{c}_j|, \sigma_c) g(|\mathbf{n}_i - \mathbf{n}_j|, \sigma_s),$$

where  $a_j$  is the area of the corresponding element. The term  $f(|\mathbf{c}_i - \mathbf{c}_j|, \sigma_c)$  and  $g(|\mathbf{n}_i - \mathbf{n}_j|, \sigma_s)$  represent the closeness and the similarity functions respectively. The kernel width of these functions are controlled by  $\sigma_c$  and  $\sigma_s$  respectively. The centroid of an element is represented by  $\mathbf{c}$ .

### Robust Estimation

The problem of the estimation of a smooth surface from a noisy surface can be written by using the tools of robust statistics. As shown by Black et al. [13], Durand et al. [14] and Jones et al. [16], to compute a smooth surface, Equation (1) can be written as the following minimization problem:

$$\min_{\mathbf{n}_i} \sum_{j \in \Omega_i} a_j f(|\mathbf{c}_i - \mathbf{c}_j|, \sigma_c) \rho(|\mathbf{n}_i - \mathbf{n}_j|, \sigma_s), \quad (2)$$

where  $\rho$  is a robust error norm [28]. The minimization of the above function will lead to smooth face normals. To solve Equation (2), the first derivative of the  $\rho$ -function should be zero which is a so-called *influence function*  $\Psi(x, \sigma_s) = \rho'(x, \sigma_s)$ , where  $x$  can be any variable (in our algorithm  $x = (\mathbf{n}_i - \mathbf{n}_j)$ ). The influence function shows the behaviour of a  $\rho$ -function.

For anisotropic diffusion and bilateral filtering, the influence function  $\Psi(x, \sigma_s)$  and  $\rho(x, \sigma_s)$ -function can be written in terms of the similarity function  $g(x, \sigma_s)$  [14]:

$$\Psi(x, \sigma_s) = xg(x, \sigma_s), \quad \rho(x, \sigma_s) = \int xg(x, \sigma_s) dx.$$

The selection of a  $\rho$ -function will be crucial to avoid outliers. In our framework, the outliers will be sharp features and an appropriate  $\rho$  function will help the algorithm to retain sharp features and remove noise components.

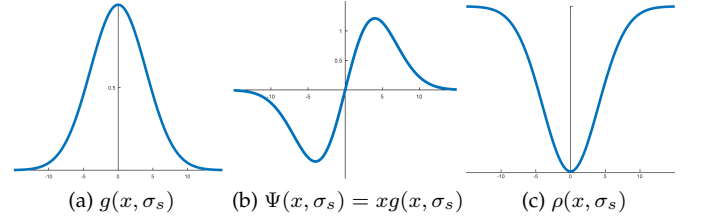


Figure 1: A Gaussian-based similarity function and corresponding influence function and  $\rho$ -function [13].

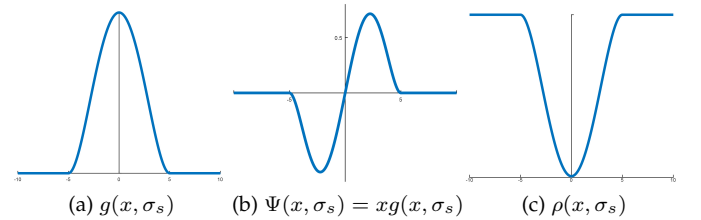


Figure 2: Tukey bi-weight similarity function and corresponding influence function and  $\rho$ -function [13].

For example, the least square estimator (a quadratic  $\rho$ -function) will be the most naive estimator because it will have a linear influence function without any bounds and will be very sensitive to outliers. Figure 1 shows the Gaussian-based  $\rho$ -function which has a bounded influence function  $\Psi(x)$  and gives smaller weight to outliers compared to the least square estimators. Figure 2 shows that *Tukey's bi-weight function* produces more robust results compared to the least square and Gaussian-based estimators



because it completely cuts off the diffusion at sharp features (outliers) and removes noise from non-feature areas. *Tukey's bi-weight function* is defined as [13]:

$$g(x, \sigma_s) = \begin{cases} \frac{1}{2} \{1 - (x/\sigma_s)^2\}^2 & \text{if } |x| \leq \sigma_s, \\ 0 & \text{if } |x| > \sigma_s. \end{cases} \quad (3)$$

In terms of preserving features, *Tukey's bi-weight function* is more effective compared to the Gaussian function because it does not allow the diffusion across sharp features and removes noise components along sharp features effectively. In our algorithm, we use *Tukey's bi-weight function* as the similarity function to produce feature preserving smooth face normals. For the closeness function  $f(\mathbf{c}_i - \mathbf{c}_j, \sigma_c)$ , a Gaussian function is used.

## 2.2 High Fidelity Mesh Reconstruction

In the second step of the denoising process, we need to impose the effect of processed face normals to the corresponding vertices. To reconstruct a high fidelity mesh, we minimize the following quadratic energy function:

$$\min_{\mathbf{v}_i} \left\{ \|\mathbf{v}_i - \tilde{\mathbf{v}}_i\|^2 + \sum_{j=0}^{N_v(i)-1} \sum_{(i,j) \in \partial F_k} \|\tilde{\mathbf{n}}_k \cdot (\mathbf{v}_i - \mathbf{v}_j)\|^2 + \|\mathbf{D}_i + \mathbf{D}_{t_i}\|^2 \right\}, \quad (4)$$

where  $\tilde{\mathbf{v}}_i$  is the newly computed vertex position. The terms  $N_v(i)$  and  $\partial F_k$  represent the number of vertices and the boundary edge of the vertex star of  $\mathbf{v}_i$  respectively. The second term of the energy function synchronizes a vertex position to the corresponding element normal by using the concept of orthogonality between edge vector and face normal [29]. The last term is an isotropic term based on the

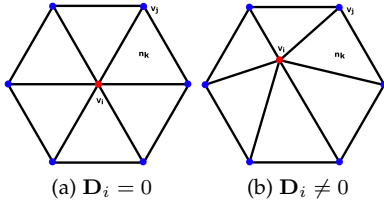


Figure 3: An example to show the effect of differential coordinate  $\mathbf{D}_i$  at the second stage of the proposed algorithm.

differential coordinate and produces a high fidelity mesh. This term makes the proposed algorithm robust against high intensity noise.

The term  $\mathbf{D}_i$  represents the differential coordinate at the vertex  $\mathbf{v}_i$  and is defined as:

$$\mathbf{D}_i = \Delta \mathbf{v}_i - \mathbf{v}_i, \quad (5)$$

where

$$\Delta \mathbf{v}_i = \frac{1}{\sum_{j \in N(i)} w_{ij}} \sum_{j \in N(i)} w_{ij} \mathbf{v}_j. \quad (6)$$

The weighting term is defined as  $w_{ij} = \|\mathbf{v}_i - \mathbf{v}_j\|^2$ , which is basically based on the edge length of connected vertices.

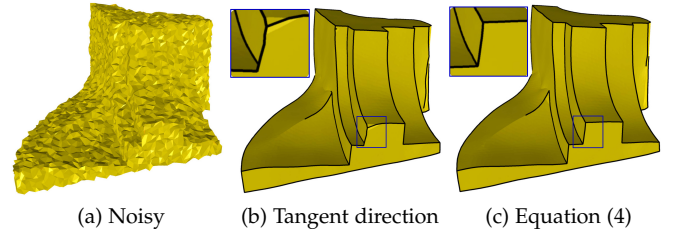


Figure 4: The Fandisk model corrupted by a uniform noise ( $\sigma_n = 0.65l_e$ ) in random direction where  $l_e$  is the average edge length. Figure (b) and (c) show effect of the diffusion of  $\mathbf{D}_i$  only in the tangent direction and using Equation (4) respectively. The sharp feature curve (black curve) is computed using the dihedral angle ( $\theta = 35^\circ$ ). The magnified view shows that the diffusion only in tangent direction is not able to reconstruct the sharp corner.

As shown in Figure 3, the differential coordinate  $\mathbf{D}_i$  computes the deviation vector from the centroid of the 1-ring neighbour to compute a high fidelity mesh.

In Equation (4), the term  $\mathbf{D}_{t_i}$  represents the tangential component of the differential coordinate  $\mathbf{D}_i$  w.r.t. the average vertex normal within the 1-ring neighbour. To compute the components of a differential coordinate along the normal and the tangent directions of the 1-ring neighbourhood, we need to approximate the vertex normal for the 1-ring, which is computed as:

$$\bar{\mathbf{n}}_{v_i} = \text{Normalized} \left( \mathbf{n}_{v_i} + \sum_{j \in N_v(i)} \mathbf{n}_{v_j} \right), \quad (7)$$

where  $\mathbf{n}_{v_i}$  represents the vertex normal at a vertex  $\mathbf{v}_i$ . Now by using this 1-ring surface normal, the differential coordinate component in the tangent direction is computed as:

$$\mathbf{D}_{t_i} = \mathbf{D}_i - \langle \mathbf{D}_i, \bar{\mathbf{n}}_{v_i} \rangle \bar{\mathbf{n}}_{v_i}, \quad (8)$$

where the term  $\langle \mathbf{D}_i, \bar{\mathbf{n}}_{v_i} \rangle \bar{\mathbf{n}}_{v_i}$  represents the component of the differential coordinate in the vertex normal direction. The normal component of the differential coordinate will be more effective against high intensity noise because mostly noise effects in the surface normal direction. Diffusion only in normal direction leads to more shrinkage because the shape information of a geometry is embedded in the surface normal. Similarly, diffusion of the tangential components leads to the better mesh quality, less shrinkage, and shape deformation, but it is less effective against high intensity noise. Figure 4 shows the effect of diffusion only in tangent direction and another one by using the equation (4). As it can be seen, the diffusion along the tangent and the normal directions produces a better result compared to the diffusion only in the tangent direction.

Minimization of energy function mentioned in equation (4) can be done by the gradient descent method and the updated vertex position will be:

$$\tilde{\mathbf{v}}_i = \mathbf{v}_i + \frac{1}{3F(\mathbf{v}_i)} \sum_{j=0}^{N_v(i)-1} \sum_{(i,j) \in \partial F_k} (\tilde{\mathbf{n}}_k \cdot (\mathbf{v}_i - \mathbf{v}_j)) + \lambda_I (\mathbf{D}_i + \mathbf{D}_{t_i}), \quad (9)$$

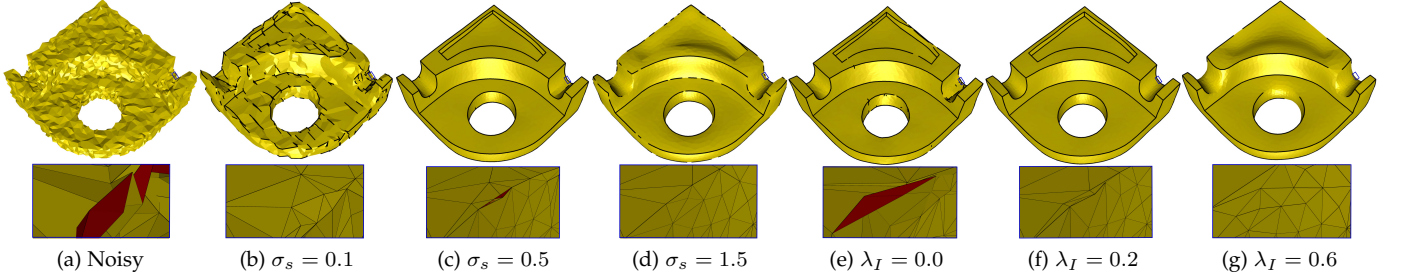


Figure 5: The Bearing model is corrupted with an uniform noise ( $\sigma_n = 0.5l_e$ ) in random direction (a). For Figure (b)-(d),  $\lambda_I = 0.02$  and for Figure (e)-(g),  $\sigma_s = 0.8$ . The black curve shows the sharp edge information in the smooth geometry and is detected using the dihedral angle  $\theta = 65^\circ$ . The second row shows the magnified view mesh structure at a sharp edge. The red color elements are with wrong orientation (flipped normals).

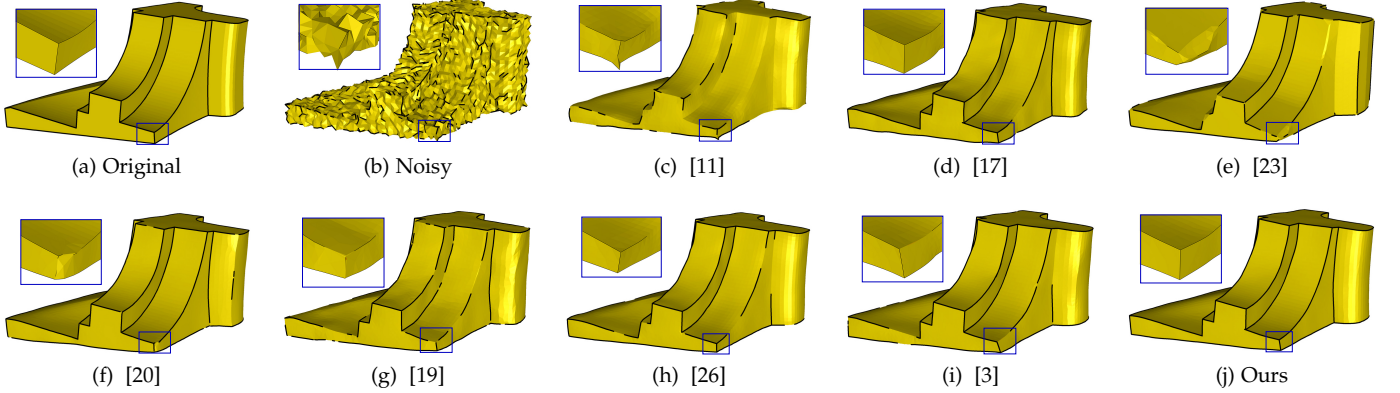


Figure 6: Fandisk model corrupted with a Gaussian noise ( $\sigma_n = 0.3l_e$ ) in random direction. The first row shows the results produced by state-of-the-art methods and our proposed method. The black curve shows the sharp edge information in the smooth geometry and is detected using the dihedral angle  $\theta = 70^\circ$ .

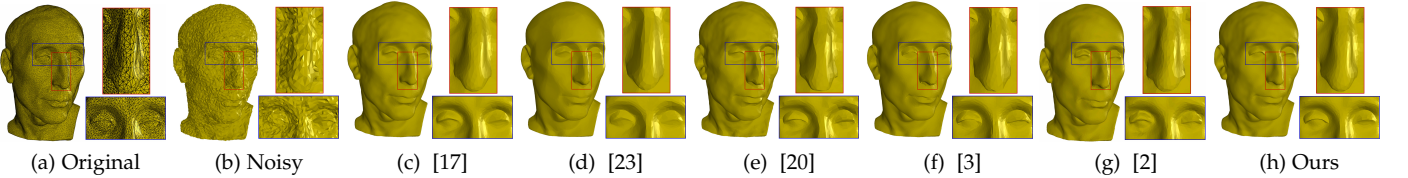


Figure 7: The Nicola model, a non-uniform triangulated mesh surface corrupted by Gaussian noise in random direction. The magnified view of the eyes and the nose shows that the proposed method preserves better sharp features without creating piecewise flat areas compared to state-of-the-art methods.

where  $F(v_i)$  represents the number of elements connected to the vertex  $\mathbf{v}_i$  and  $\lambda_I$  is the isotropic smoothing or mesh fidelity factor. We iterate the whole procedure mentioned in Equation (9) several times to get the desired result. In each iteration, using the same value of  $\lambda_I$  leads to feature blurring, shape deformation and volume shrinkage in the smoothed surface as noise is getting lower with the iterations. To overcome this problem, the effect of isotropic smoothing should get reduced after each iteration. We reduce  $\lambda_I$  in every iteration by  $\lambda_I^{p+1} = 0.6\lambda_I^p$ , where  $p$  represents the number iterations.

### 3 EXPERIMENTS, RESULTS AND DISCUSSION

We have performed our denoising scheme on various kinds of CAD (Figure 4, 5, 6, 8 and 9) and CAGD (Figure 7, 9 and 10) models. These models consist of different levels of features and are corrupted with different kind of synthetic noise (Gaussian and uniform) in different random directions. We also included real scanned data (Figure 11, 12 and 13) models in our experiments. We provide the visual and quantitative comparison of our method to several state-of-the-art denoising methods in which we implemented [3], [15], [17], [11] and [23] based on their published article and several results of [2], [19], [20], [30] and [26] are provided by their authors.

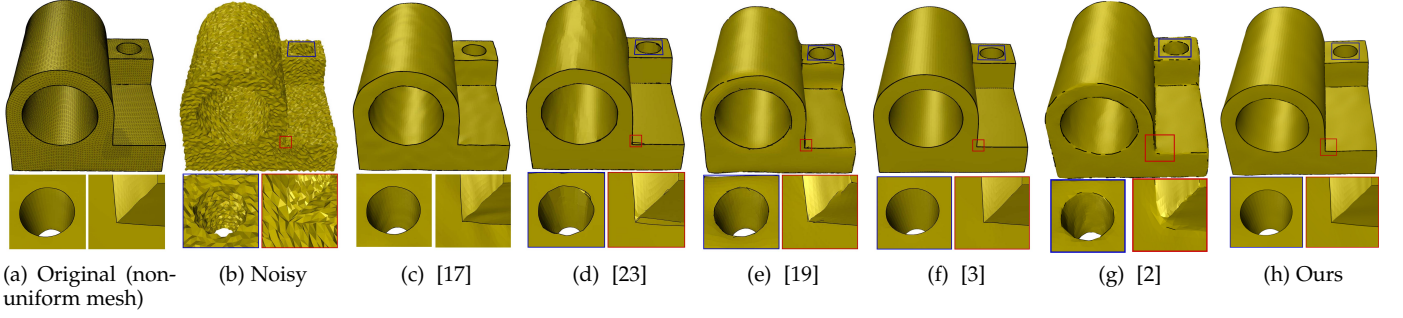


Figure 8: Non-uniform triangulated mesh surface corrupted by Gaussian noise ( $\sigma_n = 0.35l_e$ ) in normal direction. The first row shows the results obtained by state-of-the-art methods and the proposed method. The second row shows the magnified view of the corner and the cylindrical hole of the corresponding geometry.

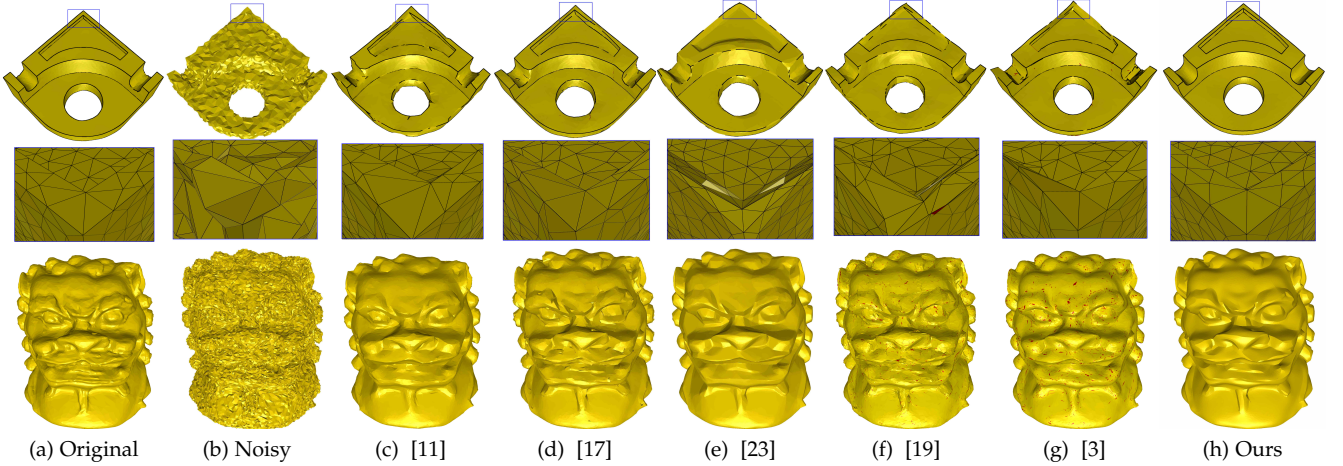


Figure 9: Figure (a) shows the noisy models, which are corrupted by a uniform noise ( $\sigma_n = 0.5l_e$ ) in random directions. Figure (b)-(h) show the results produced by state-of-the-art methods and the proposed method. The second row shows the magnified view of the mesh quality at the sharp corners. The sharp feature curves are computed at  $\theta = 65^\circ$  (for the Bearing model) and the red color elements are with wrong orientation (flipped normals).

### 3.1 Parameters

In the proposed method, we discussed about five different parameters: kernel widths of the closeness and similarity functions ( $\sigma_c$  and  $\sigma_s$ ), geometric neighbour disk ( $\Omega$ ), isotropic/mesh fidelity factor  $\lambda_I$  and the number of iterations  $p$ . Throughout the algorithm, the radius of the neighbour disk is defined as  $r = 2c_a$ , where  $c_a$  represents the average distance between the centroid of elements and the kernel width of the closeness function is half of the radius of the neighbour disk ( $\sigma_c = c_a$ ). The average centroid distance-based radius will make the algorithm robust against irregular sampling as the denser region will have more elements compared to the rare region during the face normal processing. Effectively, the user has to tune only 3 parameters ( $\sigma_s$ ,  $\lambda_I$  and  $p$ ) to get the desired results. In the quantitative comparison table, the proposed method parameters are mentioned in the following format ( $\sigma_s, \lambda_I, p$ ). Similarly, ( $\tau, r, p$ ) for [3], where  $\tau$  is the feature threshold,  $r$  is the radius of the geometric neighborhood disk and  $p$  is the number of iterations. The parameters ( $\sigma_c, \sigma_s, p$ ) for [15], ( $\sigma_s, p$ ) for [17], ( $\lambda, s, p$ ) for [11] and ( $\alpha$ ) for [23],

where  $\sigma_c$  and  $\sigma_s$  are the standard deviation of the Gaussian function in the bilateral weighting. The variables  $s$  and  $\lambda$  represent the step size and the smoothing threshold. The term  $\alpha$  controls the amount of smoothing in [23].

Figure 5 shows the effect of the kernel width parameter ( $\sigma_s$ ) of the similarity function and isotropic factor ( $\lambda_I$ ). The black curve represents sharp features and is computed using the dihedral angle ( $\theta = 65^\circ$ ) between neighboring faces. From Figure 5 (b-d), the isotropic factor is fixed ( $\lambda_I = 0.02$ ). The small value of the  $\sigma_s = 0.1$  produces a piecewise flat region and is not able to produce a noise free surface with sharp features (Figure 5 (b)). For  $\sigma_s = 1.5$ , it smooths out the sharp features and for  $\sigma_s = 0.5$ , the algorithm produces a quite optimal result. Similarly, from Figure 5 (e-g), the parameter  $\sigma_s$  is fixed ( $\sigma_s = 0.8$ ). For  $\lambda_I = 0$ , we can see that the reconstructed surface has several edge flips (elements with wrongly oriented normals) and the algorithm is not able to preserve all desired features (Figure 5(e)). However, the algorithm produces a high fidelity mesh with sharp features when we use  $\lambda_I = 0.2$  (Figure 5(f)) and blurs the sharp features with bigger isotropic factor (Figure 5 (g)). In general, the value of  $\lambda_I$  depends on noise intensity on



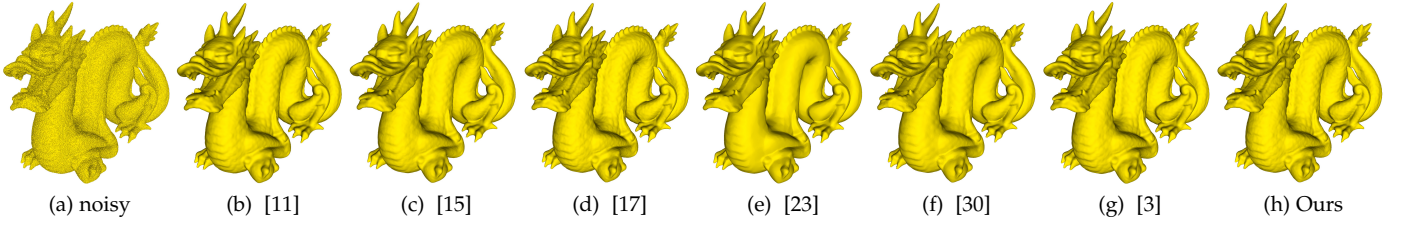


Figure 10: The Dragon model corrupted by a Gaussian noise random direction. Figure shows that the proposed method produces better results compared to Method [15], [11], [30], [23] and similar to Method [17] and [3].

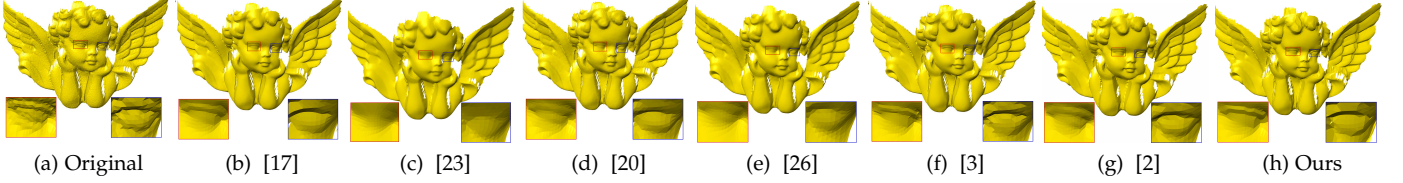


Figure 11: The Angel model, a triangulated mesh surface (real data) obtained by a 3D scanner. The figures shows the result produced by the proposed method, better preserving sharp features (both eyes) compared to state-of-the-art methods.

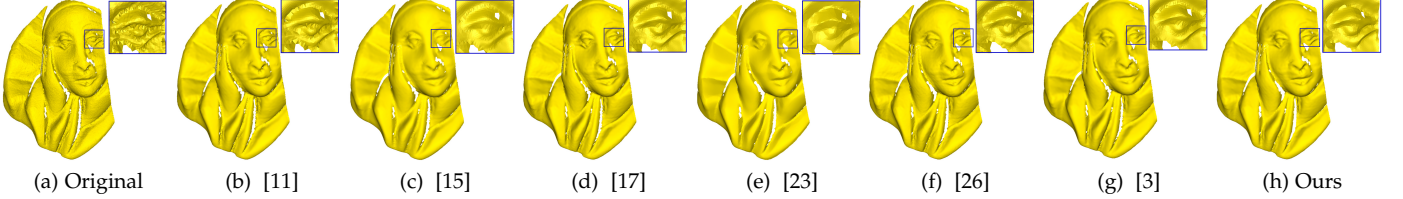


Figure 12: The Pierrot model (real data) is corrupted by a 3D scanner noise. The figures shows the results obtained by state-of-the-art methods and the proposed method.

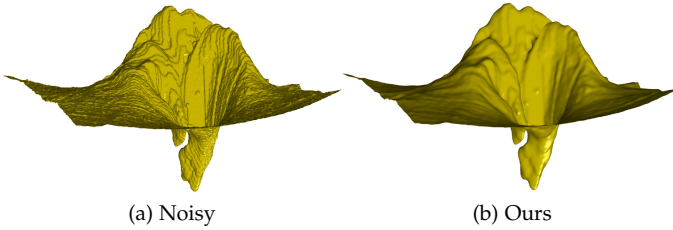


Figure 13: Figure (a) shows the noisy model of a human retina with marching cube artifacts and the proposed method removes these artifacts and noise effectively.

surfaces. The higher the intensity of noise the more normal flips will be produced during the denoising process, so it is better to use a bigger value of  $\lambda_I$  to avoid these normal flips. At the same time, we need to be careful with a bigger value of  $\lambda_I$  as it can produce edge blurring and volume shrinkage.

### 3.2 Visual Comparison

Figure 6-12 serve the purpose of visual comparison of the proposed method with several state-of-the-art methods. Figure 6 shows the Fandisk model which is corrupted with a moderate intensity Gaussian noise in random direction. The

sharp feature curve (black curve) shows that the proposed method preserves sharp features (especially at corners) effectively and does not produce false features at the cylindrical region compared to state-of-the-art methods. Method [3] and [26] manage to produce features at sharp corners but do not recover the sharp features on the whole surface. Method [23] creates false features at the cylindrical region and is not able to preserve the corner features [2]. The Nicola model (Figure 7) has a non-uniform mesh and is corrupted by a Gaussian noise in random direction. The magnified view shows that our method preserves sharp features around the eye regions better than state-of-the-art methods and does not produce any false features around the nose area (piecewise flat areas). Figure 8 shows the Joint sharp model with non-uniform mesh corrupted with a Gaussian noise ( $\sigma_n = 0.35l_e$ ) in normal direction. As it is shown, the proposed method reconstructs the cylindrical region and corners without creating any false features. Method [3] produces a quite similar result to ours while Method [20] and [23] produce false features around the cylindrical region. The other state-of-the-art methods are not able to preserve sharp features. Figure 9 provides the visual comparison between state-of-the-art methods and the proposed method where models are corrupted with high intensity of noise ( $\sigma_n = 0.5l_e$ ). As it is shown in Figure 9, our method is able to remove noise components properly and retains the sharp features

without creating any edge flips. Somehow, Method [17] is able to preserve sharp features but produces edge flips and the mesh quality is not optimal. Method [23] is also using an isotropic regularization factor which helps the algorithm to produce a good quality mesh on the planar areas but fails to produce the same near the sharp edges (second row Figure 9(c)). The Dragon model is shown in Figure 10 which is corrupted by a Gaussian noise in random direction. The proposed method produces a better result compared to Methods [30], [23], [11] and [15] and a quite similar to Methods [3] and [17].

In general, real data are captured using the 3D scanners and have quite low intensity of noise. So we can not see the considerable difference between the results of the proposed method and state-of-the-art methods. Figure 11 shows that our algorithm better preserves feature around both eyes compared to state-of-the-art methods. Methods [3] and [17] are able to retain the feature in the right eye but fail for the left eye. The other state-of-the-art methods are not able to preserve the fine level of features in both eyes. In case of the Pierrot model (Figure 12), our method removes noise effectively around the eyes and preserves features. Methods [26] and [3] retain similar scale of the feature but are not able to remove noise properly. Figure 13 shows the applicability of the proposed method to the medical data. Figure 13(a) shows a noisy model of human retina obtained by the optical coherence tomography [31] and the surface has the marching cube artifacts which is removed by the proposed method along with noise components effectively.

Table 1: Quantitative Comparison

Models	Methods	MSAE	$E_v \times 10^{-3}$	$Q$	Parameters
Nicola $ F  = 29437$ $ V  = 14846$	[15]	7.45	172.7	1.18	(0.3, 0.3, 30)
	[11]	6.269	76.87	1.00	(0.05, 0.05, 50)
	[17]	<b>5.25</b>	<b>66.07</b>	1.02	(0.3, 60)
	[23]	6.50	99.58	0.91	(1.4)
	[20]	5.82	69.63	1.05	(Default)
	[3]	5.900	72.8	1.02	(0.3, 0.15, 50)
	<b>Ours</b>	5.5	66.14	<b>0.9</b>	(1.6, 0.06, 25)
Bearing $ F  = 6950$ $ V  = 3475$	[17]	3.17	0.590	1.45	(0.3, 50)
	[23]	4.70	1.24	1.58	(4.0)
	<b>Ours</b>	<b>2.32</b>	<b>0.588</b>	<b>0.74</b>	(0.8, 0.2, 100)
Joint $ F  = 52226$ $ V  = 26111$	[15]	3.777	0.530	0.83	(0.3, 0.3, 40)
	[11]	2.630	0.766	0.78	(0.009, 0.05, 50)
	[17]	1.808	0.263	0.77	(0.4, 100)
	[23]	1.768	0.500	0.75	(1.4)
	[20]	0.956	0.179	0.83	(Default)
	[19]	2.874	0.366	1.67	(Default)
	[26]	1.16	1.49	<b>0.71</b>	(Default)
	[3]	<b>0.829</b>	<b>0.171</b>	0.91	(0.3, 0.05, 60)
	<b>Ours</b>	1.032	0.198	0.73	(1.0, 0.2, 150)
Fandisk $ F  = 12946$ $ V  = 6475$	[15]	8.567	4.422	0.87	(0.4, 0.4, 40)
	[11]	5.856	4.910	0.79	(0.07, 0.05, 30)
	[17]	2.727	1.877	0.76	(0.4, 70)
	[23]	4.788	5.415	0.766	(1.4)
	[20]	2.221	<b>1.702</b>	0.97	(Default)
	[26]	3.1	4.42	0.7	(Default)
	[3]	2.692	1.964	0.89	(0.3, 0.2, 50)
	<b>Ours</b>	<b>2.201</b>	1.844	<b>0.7</b>	(0.55, 0.2, 100)
Chinese Lion $ F  = 118276$ $ V  = 59140$	[17]	14.88	19.64	2.72	(1.0, 100)
	[23]	8.93	25.34	1.51	(1.4)
	<b>Ours</b>	<b>8.795</b>	<b>18.35</b>	<b>0.85</b>	(0.4, 0.3, 100)
Sharp Sphere $ V  = 3827$ $ F  = 7650$	[17]	<b>8.73</b>	21.65	2.40	(Default)
	[23]	8.59	30.28	1.25	(1.6)
	<b>Ours</b>	<b>8.39</b>	<b>21.62</b>	<b>0.78</b>	(0.5, 0.2, 100)

### 3.3 Quantitative Comparison

For the quantitative comparison, we are using three different parameters. Basically, two of them show the differences between the ground truth and smooth model and so-called  $L^2$  vertex-based positional error and the orientation error respectively. The third parameter computes the mesh quality of a smoothed surface. The  $L^2$  vertex-based positional

error from the original ground truth model is represented by  $E_v$  and defined as [32]:

$$E_v = \sqrt{\frac{1}{3 \sum_{k \in F} a_k} \sum_{i \in V} \sum_{j \in F_v(i)} a_j \text{dist}(\tilde{\mathbf{v}}_i, T)^2},$$

where  $F$  is the triangular element set and  $V$  represents the set of vertices. The terms  $a_k$  and  $a_j$  are the corresponding element areas and  $F_v(i)$  is the number of elements in the  $i^{th}$  vertex-ring. The distance  $\text{dist}(\tilde{\mathbf{v}}_i, T)$  is the closest  $L^2$ -distance between the newly computed vertex  $\tilde{\mathbf{v}}_i$  and the triangle  $T$  of the reference model.

The MSAE computes the orientation error between the original model and the smooth model and is defined as:

$$\text{MSAE} = E[\angle(\tilde{\mathbf{n}}, \mathbf{n})],$$

where  $\tilde{\mathbf{n}}$  is the newly computed face normal and  $\mathbf{n}$  represents the face normal of the reference model. The term  $E$  stands for the expectation value.

Mesh quality of the surface is mainly referred to the shape of the elements in the mesh. For a better mesh quality, the size and angles of the triangular element should not be too small or large. To measure the quality of elements, we use the ratio of the circumradius-to-minimum edge length of the corresponding element [33]:

$$Q = \frac{r}{e_{min}},$$

where  $r$  and  $e_{min}$  are circumradius and minimum edge length of the corresponding triangle. Ideally, every element belonging to the mesh should be an equilateral triangle with a quality index of  $Q = 1/\sqrt{3}$ .

Table 1 shows the quantitative comparison of our method with state-of-the-art methods. For the models which are corrupted with high intensity (Bearing, Chinese Lion and Sharp Sphere), the proposed method lower values of  $E_v$ , MSAE and  $Q$  compared to Methods [17] and [23]. Method [17] produces a quite similar value of  $E_v$  but bigger values for MSAE and  $Q$  because of the several edge flips. He et al. [23] produces a quality mesh in planar region but fails to similar quality of triangle near sharp features and that leads to a higher value mesh quality index. For the Nicola model, our method produces a quite similar value of the position and orientation error (slightly bigger) to Method [17], because our algorithm also follows the bilateral filtering technique and in addition, we use an isotropic factor which introduces a bit of volume shrinkage. At the same time, it produces a good quality mesh. Similarly, Method [3] uses an isotropic operator in initial estimation which helps them to produce a quite similar mesh quality with the Joint and the Fandisk models.

### 3.4 Running Time

As it is explained by [3], the two step denoising methods have quite similar running time complexity. The proposed algorithm also follows the two step denoising scheme and has the complexity of  $O(c \cdot n_f \cdot p)$ , where  $c$  is the number of elements within the neighbourhood,  $n_f$  and  $p$  are the numbers of elements and iterations respectively.

Table 2: Running Time (in seconds)

Models	Fandisk	Bearing	Nicola	Joint	Lion
Time (s)	5.8	4.2	4.3	45.3	92

The implementation of the algorithm is quite straightforward and simple. First of all, we compute the smooth face normals using Equation (1) and then rearrange vertices by following the Equation (9). Our implementation is done in a single computation thread using Java. Table 2 shows the running time of our algorithm for different models according to the parameter values mentioned in Table 1.

#### 4 CONCLUSION

In this paper, we presented a robust mesh denoising algorithm which produces a high quality mesh along with sharp features. In the first step of the proposed method, a robust statistics framework is applied for noisy face normal smoothing where *Tukey's bi-weight function* is used as the robust estimator. *Tukey's bi-weight function* completely stops the diffusion across sharp edges and removes noise along the sharp features and from flat areas. In the second step, a vertex position is updated using face normal-edge orthogonality constraints along with differential coordinates. Differential coordinates helps the algorithm to produce a high quality mesh, makes it robust against high intensity of noise and avoids normal flips during the denoising process. The quantitative comparison table shows that our method produces better mesh quality compared to state-of-the-art methods. Similarly, for the positional and the orientation error, the proposed method is either better or similar to state-of-the-art methods.

#### REFERENCES

- [1] M. Botsch, L. Kobbelt, M. Pauly, P. Alliez, and B. uno Levy, *Polygon Mesh Processing*. AK Peters, 2010.
- [2] M. Centin and A. Signoroni, "Mesh denoising with (geo)metric fidelity," *IEEE Transactions on Visualization and Computer Graphics*, vol. PP, no. 99, pp. 1–1, 2017.
- [3] S. K. Yadav, U. Reitebuch, and K. Polthier, "Mesh denoising based on normal voting tensor and binary optimization," *IEEE Transactions on Visualization and Computer Graphics*, vol. PP, no. 99, pp. 1–1, 2017.
- [4] M. Alexa, "Differential coordinates for local mesh morphing and deformation," *The Visual Computer*, vol. 19, no. 2-3, pp. 105–114, 2003.
- [5] Y. Lipman, O. Sorkine, M. Alexa, D. Cohen-Or, D. Levin, C. Rössl, and H.-P. Seidel, "Laplacian framework for interactive mesh editing," *International Journal of Shape Modeling (IJSM)*, vol. 11, no. 1, pp. 43–61, 2005.
- [6] O. Sorkine, D. Cohen-Or, and S. Toledo, "High-pass quantization for mesh encoding," in *Proceedings of the 2003 Eurographics/ACM SIGGRAPH Symposium on Geometry Processing*, ser. SGP '03. Aire-la-Ville, Switzerland, Switzerland: Eurographics Association, 2003, pp. 42–51.
- [7] O. Sorkine, D. Cohen-Or, D. Irony, and S. Toledo, "Geometry-aware bases for shape approximation," *IEEE Transactions on Visualization and Computer Graphics*, vol. 11, no. 2, pp. 171–180, Mar. 2005.
- [8] O. Sorkine, "Differential representations for mesh processing," *Computer Graphics Forum*, vol. 25, no. 4, pp. 789–807, 2006.
- [9] Z.-X. Su, H. Wang, and J.-J. Cao, "Mesh denoising based on differential coordinates," in *Shape Modeling and Applications, 2009. SMI 2009. IEEE International Conference on*, June 2009, pp. 1–6.
- [10] C. Tomasi and R. Manduchi, "Bilateral filtering for gray and color images," in *Proceedings of the Sixth International Conference on Computer Vision*, ser. ICCV '98. Washington, DC, USA: IEEE Computer Society, 1998, pp. 839–846.
- [11] K. Hildebrandt and K. Polthier, "Anisotropic filtering of non-linear surface features," *Computer Graphics Forum*, vol. 23, pp. 391–400, 2004.
- [12] D. Barash, "Fundamental relationship between bilateral filtering, adaptive smoothing, and the nonlinear diffusion equation," *Pattern Analysis and Machine Intelligence, IEEE Transactions on*, vol. 24, no. 6, pp. 844–847, Jun 2002.
- [13] M. J. Black, G. Sapiro, D. H. Marimont, and D. Heeger, "Robust anisotropic diffusion," *IEEE Transactions on Image Processing*, vol. 7, no. 3, pp. 421–432, Mar 1998.
- [14] F. Durand and J. Dorsey, "Fast bilateral filtering for the display of high-dynamic-range images," in *Proceedings of the 29th Annual Conference on Computer Graphics and Interactive Techniques*, ser. SIGGRAPH '02. New York, NY, USA: ACM, 2002, pp. 257–266.
- [15] S. Fleishman, I. Drori, and D. Cohen-Or, "Bilateral mesh denoising," in *ACM SIGGRAPH 2003 Papers*, ser. SIGGRAPH '03. New York, NY, USA: ACM, 2003, pp. 950–953.
- [16] T. R. Jones, F. Durand, and M. Desbrun, "Non-iterative, feature-preserving mesh smoothing," *ACM Trans. Graph.*, vol. 22, no. 3, pp. 943–949, Jul. 2003.
- [17] Y. Zheng, H. Fu, O.-C. Au, and C.-L. Tai, "Bilateral normal filtering for mesh denoising," *Visualization and Computer Graphics, IEEE Transactions on*, vol. 17, no. 10, pp. 1521–1530, Oct 2011.
- [18] J. Solomon, K. Crane, A. Butscher, and C. Wojtan, "A general framework for bilateral and mean shift filtering," *ArXiv e-prints*, vol. 32, April 2014.
- [19] M. Wei, J. Yu, W. M. Pang, J. Wang, J. Qin, L. Liu, and P. A. Heng, "Bi-normal filtering for mesh denoising," *IEEE Transactions on Visualization and Computer Graphics*, vol. 21, no. 1, pp. 43–55, Jan 2015.
- [20] W. Zhang, B. Deng, J. Zhang, S. Bouaziz, and L. Liu, "Guided mesh normal filtering," *Computer Graphics Forum (Special Issue of Pacific Graphics 2015)*, vol. 34, pp. 23–34, 2015.
- [21] J. Kopf, M. F. Cohen, D. Lischinski, and M. Uyttendaele, "Joint bilateral upsampling," *ACM Trans. Graph.*, vol. 26, no. 3, Jul. 2007.
- [22] M. Wei, L. Liang, W. M. Pang, J. Wang, W. Li, and H. Wu, "Tensor voting guided mesh denoising," *IEEE Transactions on Automation Science and Engineering*, vol. 14, no. 2, pp. 931–945, April 2017.
- [23] L. He and S. Schaefer, "Mesh denoising via  $L^0$  minimization," *ACM Trans. Graph.*, vol. 32, no. 4, pp. 64:1–64:8, Jul. 2013.
- [24] R. Wang, Z. Yang, L. Liu, J. Deng, and F. Chen, "Decoupling noise and features via weighted  $L^1$ -analysis compressed sensing," *ACM Trans. Graph.*, vol. 33, no. 2, pp. 18:1–18:12, Apr. 2014.
- [25] X. Wu, J. Zheng, Y. Cai, and C.-W. Fu, "Mesh Denoising using Extended ROF Model with L1 Fidelity," *Computer Graphics Forum*, 2015.
- [26] X. Lu, Z. Deng, and W. Chen, "A robust scheme for feature-preserving mesh denoising," *IEEE Transactions on Visualization and Computer Graphics*, vol. 22, no. 3, pp. 1181–1194, March 2016.
- [27] X. Lu, W. Chen, and S. Schaefer, "Robust mesh denoising via vertex pre-filtering and l1-median normal filtering," *Computer Aided Geometric Design*, vol. 54, pp. 49 – 60, 2017.
- [28] F. R. Hampel, E. M. Ronchetti, P. J. Rousseeuw, and W. A. Stahel, *Robust Statistics - The Approach Based on Influence Functions*. Wiley, 1986, missing.
- [29] G. Taubin, "Linear anisotropic mesh filtering," in *IBM Research Report RC22213(W0110-051)*, IBM T.J. Watson Research, 2001.
- [30] A. Adams, N. Gelfand, J. Dolson, and M. Levoy, "Gaussian kd-trees for fast high-dimensional filtering," in *ACM SIGGRAPH 2009 Papers*, ser. SIGGRAPH '09. New York, NY, USA: ACM, 2009, pp. 21:1–21:12.
- [31] S. K. Yadav, S. Motamedji, T. Oberwahrenbrock, F. C. Oertel, K. Polthier, F. Paul, E. M. Kadas, and A. U. Brandt, "Cube: parametric modeling of 3d foveal shape using cubic b zier," *Biomed. Opt. Express*, vol. 8, no. 9, pp. 4181–4199, Sep 2017.
- [32] X. Sun, P. Rosin, R. Martin, and F. Langbein, "Fast and effective feature-preserving mesh denoising," *Visualization and Computer Graphics, IEEE Transactions on*, vol. 13, no. 5, pp. 925–938, Sept 2007.
- [33] J. R. Shewchuk, "Delaunay Refinement Mesh Generation," Ph.D. dissertation, School of Computer Science, Carnegie Mellon University, Pittsburgh, Pennsylvania, May 1997, available as Technical Report CMU-CS-97-137.